Journal of Materials Chemistry B

ROYAL SOCIETY OF CHEMISTRY

PAPER

View Article Online
View Journal

Cite this: DOI: 10.1039/d6tb00293e

Nonionic peptide amphiphiles and their supramolecular co-assemblies tune charge density and bioactivity

Jacob A. Lewis, †‡[ab] Ronit Freeman, ‡§[b] Tristan D. Clemons, ¶[bc] Jacqueline M. Godbe, ‖[bc] Nicholas Stephanopoulos **[b] and Samuel I. Stupp *[abcde]

Supramolecular peptide assemblies generally rely on ionic groups for solubility in aqueous media but charge may sometimes affect their biological functions. Cationic residues in these assemblies are often associated with cell toxicity, and charged amino acids lead to supramolecular structures that are dependent on both pH and ionic strength. We report here on the synthesis of a nonionic peptide amphiphile (PA) containing a decaethylene glycol segment and its supramolecular co-assembly with ionic PA monomers as a strategy to produce uncharged assemblies and to fine tune charge density. We show that while morphology and internal structure depend on counterion screening and on pH for charged PA assemblies, these nonionic molecules self-assemble to form high-aspect ratio filaments containing β-sheets stable with or without ion screening and at acidic, neutral, and basic pH. By co-assembling nonionic PA molecules with charged PA molecules, we could produce supramolecular copolymers with tunable surface charge density, yet with stronger internal order than either fully charged or fully uncharged assemblies. Using an *in vitro* model for osteogenic differentiation of mesenchymal stem cells, we found that supramolecular assemblies containing nonionic molecules or co-assemblies of both nonionic and ionic PA molecules exhibit greater bioactivity than assemblies containing only charged molecules. We hypothesize that the enhanced bioactivity originates in the synergy between protein binding by PA molecules and increased supramolecular dynamics introduced by the nonionic ethylene glycol segments. Thus, nonionic PAs and their co-assemblies can be used to investigate how charge density and other factors affect bioactivity of water-soluble supramolecular nanostructures.

Received 4th February 2026,
Accepted 21st April 2026

DOI: 10.1039/d6tb00293e

rsc.li/materials-b

Introduction

It is known that electrostatic charge plays a key role in the biological activity of nanomaterials. The high interfacial energy of charged nanoscale surfaces drives adsorption of molecules,[1,2] resulting in the formation of a biomolecular corona that determines the biodistribution of nanomaterials and their interactions with specific tissues or cells.[3–5] Polyethylene glycol (PEG) is often used to coat nanomaterials and provide a hydrated uncharged polymer shell that limits the accumulation of biomolecules and prolongs bioretention.[6–8] This strategy can also enhance target recognition by decreasing signal masking by nonspecifically bound proteins and by decreasing repulsive interactions with the cell membrane.[9–11] PEGylation has been applied to self-assembling peptide-based nanomaterials, where molecular incorporation of PEG improved water solubility of hydrophobic peptides and increased order within the assemblies.[12,13] At the same time, increasing the molecular weight of the PEG chains can lead to steric repulsion among peptides and thereby increase critical micelle concentrations,[14] implying that limiting chain length is important for creating stable assemblies.

In self-assembling systems, ionic charge is especially important in determining the morphology of the supramolecular structures formed.[15–21] In addition, the charge of supramolecular assemblies determines many properties of the nanostructures including peptide

[a] *Department of Biomedical Engineering, Northwestern University, Evanston, IL 60208, USA. E-mail: stupp@northwestern.edu*
[b] *Center for Regenerative Nanomedicine, Northwestern University, Chicago, IL 60611, USA*
[c] *Department of Chemistry, Northwestern University, Evanston, IL 60208, USA*
[d] *Department of Materials Science and Engineering, Northwestern University, Evanston, IL 60208, USA*
[e] *Department of Medicine, Northwestern University, Chicago, IL 60611, USA*
† Present Address: Drug Product Technologies, Process Development, Amgen Inc., Thousand Oaks, CA, USA.
‡ These authors contributed equally.
§ Present address: Department of Applied Physical Sciences, University of North Carolina, Chapel Hill, NC, USA.
¶ Present Address: School of Polymer Science and Engineering, University of Southern Mississippi, Hattiesburg, MS, USA.
‖ Present Address: Edward Mallinckrodt Institute of Radiology, Washington University School of Medicine, St. Louis, MO, USA.
** Present address: School of Molecular Sciences, Biodesign Center for Molecular Design and Biomimetics, Arizona State University, Tempe, AZ, USA.

bioactivity,[22,23] biodistribution,[24,25] immunogenicity,[26] and gelation.[27,28] Peptide amphiphile (PA) molecules developed by our group—comprising an ionizable peptide region conjugated to an alkyl tail—are a promising platform for biomedical applications because of their highly tunable self-assembly into dynamic nanostructures with programmed morphologies such as high-aspect ratio filaments in aqueous media.[29–31] Self-assembly of these molecules leads to nanostructures with a high density of surface charge, and limiting electrostatic repulsion *via* screening of these charges by ions in the media controls the morphology of the assemblies formed.[17,32–34] In addition, the highly charged surface is known to induce apoptosis in response to cationic residues,[35] while electrostatic interactions among peptide epitopes displayed by the filament and an oppositely charged filament surface were reported to limit bioactivity of the assemblies.[15,36] It is therefore clear that charge can impact the bioactivity of self-assembling peptides and charge is essentially always present in the molecular structure of PAs. In this context, the objective of this work has been to synthesize a nonionic PA in order to more clearly understand the role of charge in its supramolecular structure. As part of the work, we also investigated systems in which nonionic and charged monomers were systematically co-assembled, evaluated the effect of uncharged PA on cell viability, and determined how PA charge affects one example of stem cell differentiation.

Results and discussion

Self-assembly of nonionic PA molecules

To produce PA filaments without ionic charge, we substituted a short PEG chain for the ionizable amino acids typically included in PA molecules for solubility in water. Previously reported filament-forming PA molecules have included oligoethylene glycol as spacers between peptide domains for self-assembly and for bioactivity[37,38] or long PEG chains to decrease degradation of PA assemblies,[39] but these molecules included ionizable peptide domains. Others have reported PA molecules where charge was limited by chemical modification of peptide side chains, producing hydrogels at low PA concentrations.[40,41] However, a significant advantage of the ionic PA molecules reported by our group is their ability to form dynamic filaments that easily dissolve in water, which has not been reported in previous studies of nonionic PAs. To form soluble, uncharged PA filaments, we chose the sequence *N*-palmitoyl-VVAA for the aliphatic tail and peptide domain, which we previously reported to form filaments with β-sheet secondary structure when the peptide domain includes ionic residues at the C-terminus, for instance *N*-palmitoyl-VVAAEE.[31] As the hydrophilic domain, we chose a decaethylene glycol amino acid to form the structure *N*-palmitoyl-VVAA-PEG_{10}-NH_2 (**PA1**, Fig. 1a and Fig. S1a). Previous work indicated an oligoethylene glycol group of this length would be short enough to limit steric repulsion among assembled molecules,[42] but we expected it would be long enough to ensure solubility and prevent protein fouling of the assemblies.[11] The PA was synthesized by coupling the PEG amino acid to a rink-amide resin and completing the peptide using standard Fmoc solid phase peptide synthesis, leaving an uncharged amide group upon cleavage. Following synthesis and purification by high-performance liquid chromatography, the molecule was readily resuspended in water, becoming slightly cloudy though without a noticeably higher viscosity at concentrations exceeding 1 wt%. We also prepared two PA molecules in which the PEG domain was replaced with either two anionic glutamic acid residues to form *N*-palmitoyl-VVAAEE-NH_2 (**PA2**,

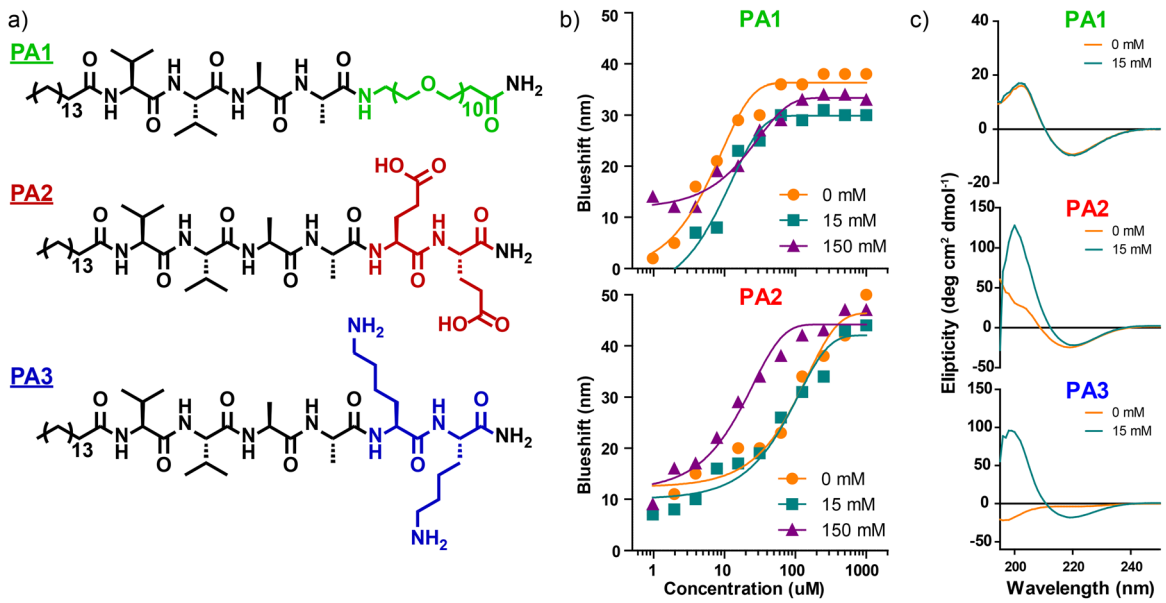

Fig. 1 (a) Structures of the uncharged **PA1**, the anionic **PA2**, and the cationic **PA3**. (b) Blueshift of peak Nile red fluorescence as a function of **PA1** or **PA2** concentration in buffers of 0 mM NaCl, 15 mM NaCl, and 150 mM NaCl. (c) CD of PA solutions plotted as a function of wavelength in 0 mM NaCl and in 15 mM NaCl.

Fig. 1a and Fig. S1b), or two cationic lysine residues to form *N*-palmitoyl-VVAAKK-NH_2 (**PA3**, Fig. 1a and Fig. S1c).

We began by assessing how the substitution of charged residues for PEGylation affected the ability of the PA molecules to self-assemble. Because **PA1** lacks ionic residues, we hypothesized its self-assembly would be less dependent on buffer salinity than its charged counterparts, as screening by ionic solutes determines the length scale of electrostatic interactions. We monitored self-assembly of the molecules using the Nile red assay, where a blueshift in the dye's fluorescence emission is correlated with the emergence of hydrophobic pockets as amphiphiles assemble.[43] Assembly of **PA1**—as indicated by the blueshift in Nile red fluorescence—occurred independently of ionic strength, while assembly of **PA2** depended on the ionic strength of the buffer, with smaller shifts recorded in 0 mM and 15 mM NaCl than in 150 mM NaCl (Fig. 1b and Table S1). For **PA3**, the blueshift in Nile red emission at high PA concentrations was about half that of **PA1** or **PA2**, suggesting less dye may have intercalated in the assemblies, making it difficult to draw conclusions from the assay (Fig. S2). To understand how charge affected the propensity of these molecules to aggregate, we used circular dichroism (CD) spectroscopy to probe the secondary structure formed by the PA solutions. CD showed that assemblies of **PA1** in solutions of 0 mM NaCl and in 15 mM NaCl had identical CD spectra consistent with β-sheet secondary structure. For **PA2**, however, a typical β-sheet signal was observed in 15 mM NaCl solution, but at 0 mM NaCl the peak centered at 200 nm was significantly diminished, suggesting the presence of random coil secondary structure in addition to β-sheet. For **PA3**, this pattern was even more pronounced with a β-sheet signal in solutions of 15 mM NaCl and only random coil signal was observed in 0 mM NaCl solutions (Fig. 1c). These results suggest that ionic screening significantly affects the secondary structure formed by **PA2** and **PA3**, which contributed to the higher aggregation concentrations recorded for **PA2**. For **PA1**, however, secondary structure is unaffected by screening and assemblies form at low concentration regardless of ionic strength. Thus, unlike charged PA molecules, the PEGylated PA reported here can self-assemble even in the absence of counterion screening.

pH dependence of PA supramolecular polymerization

We expected the nonionizable terminus of **PA1** molecules would make their supramolecular polymerization much less pH dependent than that of **PA2** and **PA3**, which contain groups that are easily deprotonated or protonated. Indeed, zeta-potential measurements confirmed that the surface charge of **PA1** filaments was approximately 0 mV at pH 2, 7, and 12, whereas the surface charges of **PA2** and **PA3** decreased at low and high pH, respectively (Fig. 2a). Cryogenic-TEM of samples

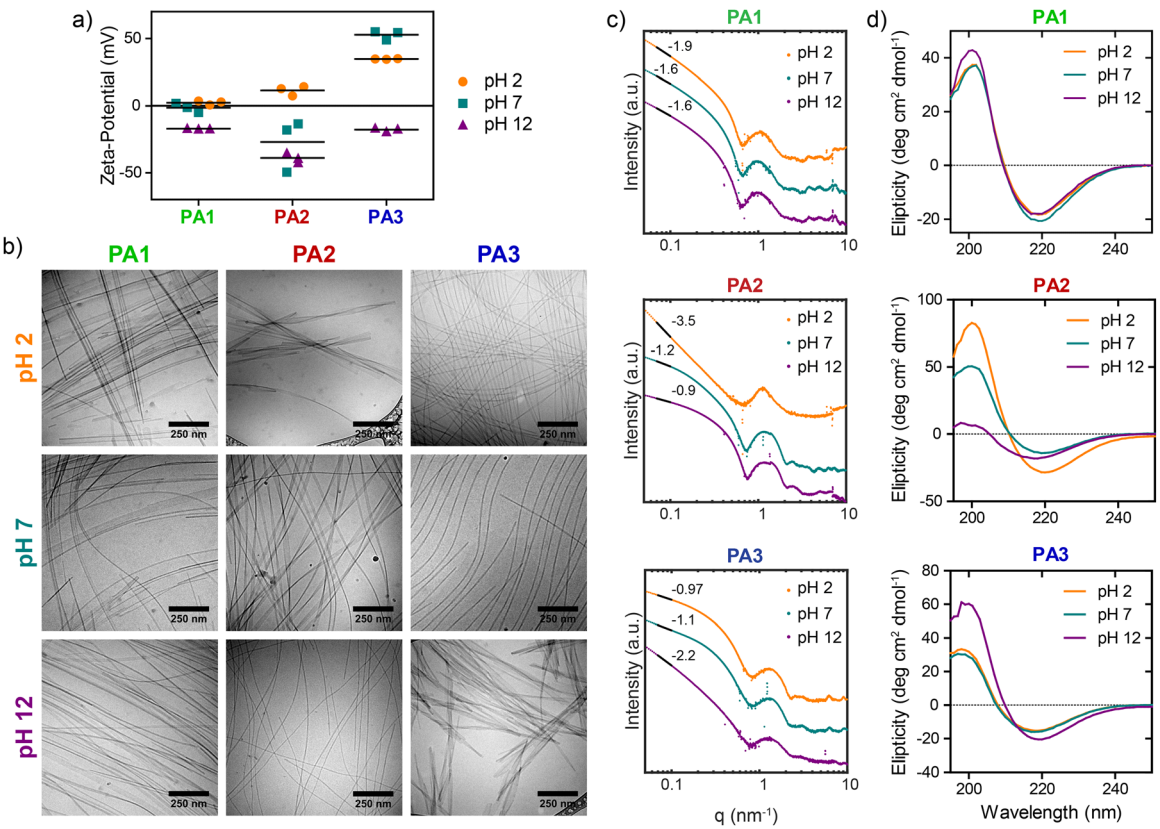

Fig. 2 (a) Zeta-potential measurements for **PA1**, **PA2**, and **PA3** solutions at pH 2, pH 7, and pH 12. (b) Cryogenic-TEM images of **PA1**, **PA2**, and **PA3** each prepared at pH 2, pH 7, and pH 12 and preserved in vitreous ice. (c) SAXS intensity as a function of the wave vector for **PA1**, **PA2**, and **PA3** solutions at pH 2, pH 7, and pH 12. (d) CD as a function of wavelength for **PA1**, **PA2**, and **PA3** solutions at pH 2, pH 7, and pH 12.

preserved in vitreous ice showed that **PA1** uniformly formed narrow ribbon structures at all pH values tested, while the morphologies observed for **PA2** and **PA3** were pH-dependent. At low pH, **PA2** formed wide, short ribbons that bundled with each other, but at and above neutral pH **PA2** formed longer, narrow fibers. Similarly, **PA3** formed wide, short, bundled structures at high pH, but formed narrow, longer filaments when charged at neutral pH and below (Fig. 2b). These observations were supported by small-angle X-ray scattering (SAXS) data, which showed little difference in the ribbon-like scattering pattern produced by **PA1** in acidic, neutral, or basic conditions, but showed a significant decrease in slope when ionic charge was increased for **PA2** and for **PA3**, consistent with a transition from planar structures to narrower filaments (Fig. 2c). We next used CD spectroscopy to determine how pH affected the secondary structure of PA molecules within the assemblies. **PA1** formed β-sheets in acidic, neutral, and basic conditions, with similar patterns observed at all three pH values. For **PA2**, β-sheet character decreased with increased pH as acidic groups were deprotonated and repelled one another. CD spectra for **PA3** were not significantly pH dependent (Fig. 2d), which we attribute to less ionization of its sidechain relative to glutamic acid. This trend is consistent with reported pK_a values for the non-assembled glutamic acid and lysine sidechains (4.3 and 10.4, respectively),[44] which based on the Henderson–Hasselbach equation implies twice as many glutamic acid residues are charged at pH 2 as lysine residues are charged at pH 12. Therefore, greater repulsion among glutamic acid residues at pH 12 may interfere with assembly more than the smaller amount of repulsion among lysine residues at pH 2.

To demonstrate that this pH-independent behavior was a result of the absence of ionic amino acid residues in **PA1** and not a general result of PEGylation alone, we synthesized two control molecules extending **PA2** and **PA3** with the 10-mer PEG amino acid to afford *N*-palmitoyl-VVAAEE-PEG_{10}-NH_2 (**PA4**, Fig. S1d and S3a) and *N*-palmitoyl-VVAAKK-PEG_{10}-NH_2 (**PA5**, Fig. S1e and S3a). Zeta-potential measurements showed that PEGylation decreased, but did not eliminate the surface charge of these molecules at neutral pH relative to their non-PEGylated counterparts. Zeta-potential was close to 0 mV only when the ionic charge was limited at pH 2 for **PA4** and pH 12 for **PA5** (Fig. S3b). SAXS showed that supramolecular polymerization of these molecules was pH dependent as observed for charged, non-PEGylated PA molecules, revealing a low-q slope that was dependent on surface charge (Fig. S4a). CD further confirmed that β-sheet formation by **PA4** and **PA5** was also pH dependent, with CD spectra showing β-sheet formation only when charge was minimal (pH 2 for **PA4** and pH 12 for **PA5**; Fig. S4b). We hypothesize that despite its short length, the addition of the PEG chain increased steric repulsion among molecules in these dense assemblies, decreasing β-sheet content. Thus, pH-independent polymerization of these PA molecules was only achieved when readily ionizable groups were absent in their chemical structure, not by merely extending their hydrophilic domain with PEG moieties. Furthermore, these results show that the uncharged **PA1** can present a PEGylated filament with β-sheet character at neutral pH, which was not possible by merely extending the charged **PA2** or **PA3** with a PEG domain.

Supramolecular copolymerization of nonionic and ionic PA molecules

In order to determine if we could tune the surface charge of PA filaments, we prepared solutions of nonionic **PA1** with anionic **PA2** by mixing solutions in a 30 mM NaCl buffer and sonicating prior to heat treatment at 80 °C for 30 min. In a previous report, the self-assembled morphology of ionic PA molecules co-assembled with nonionic, non-peptide surfactants depended on the relative concentration of the two components, which was attributed to the non-peptide surfactant disrupting hydrogen bonding among the peptide molecules.[45] In our system, both the nonionic and ionic components are peptides, allowing us to study how changing the ratio of nonionic and ionic components affects interactions among the hydrogen-bonding peptide domains. Cryogenic-TEM of the co-assemblies showed that with the addition of 5 mol% **PA2** to **PA1**, narrow ribbons formed similar to those observed in **PA1** supramolecular polymers. With the addition of 25 mol% **PA2** or higher concentrations, the resulting supramolecular filaments appeared more similar to the narrow twisting structures formed by assemblies comprised entirely of **PA2** monomers (Fig. 3a). This indicated that the charged system morphology could be achieved even with only a fraction of the molecules containing charged monomers. Consistent with this trend, SAXS showed a significant change in low-*q* slope with the addition of 25 mol% **PA2** to the uncharged **PA1** filaments, indicating a transition from wider structures to narrower assemblies. Similarly, the first minimum in the pattern—which corresponds to the diameter of the assemblies—shifted to the right as uncharged **PA1** molecules were replaced with the charged **PA2**. (Fig. 3b). Increasing the quantity of **PA2** in the assemblies from 0 mol% to 25 mol% shifted the position of the first minimum from 0.60 nm^{-1} to 0.67 nm^{-1}, while increasing **PA2** from 75 mol% to 100 mol% shifted the position of the first minimum only slightly, from 0.76 nm^{-1} to 0.77 nm^{-1}, which indicates that the incorporation of charged molecules decreased the cross-section of the assemblies. The nonlinear relationship between the fraction of charged PA molecules and the observed morphology strongly suggests that the charged and uncharged PA molecules formed supramolecular copolymers in which repulsion among charged PA monomers disrupted the nonionic PA morphology, rather than segregated assemblies. For co-assemblies of **PA1** and the cationic **PA3**, the low-*q* slope changed more gradually with the addition of charged groups (Fig. S5a), which supports the notion that electrostatic repulsion among lysine residues in neighboring β-strands affected supramolecular morphology less than repulsion among glutamic acid residues. Importantly, the transition of the scattering patterns from a **PA1**-like morphology to a **PA2**-like morphology with the addition of a small amount of **PA2** monomers indicates that only a small fraction of charged PA molecules within the assemblies is necessary to observe a transition to the morphology characteristic of charged supramolecular polymers. This suggests that once a threshold fraction of charged groups is reached in a supramolecular

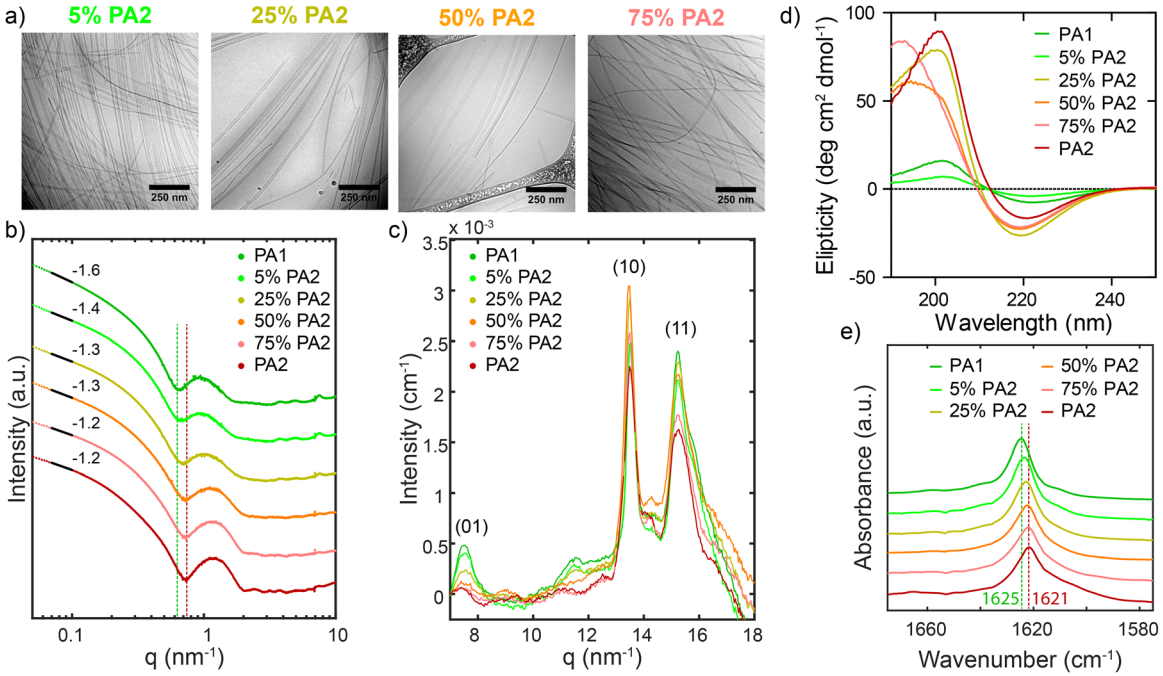

Fig. 3 (a) Cryogenic-TEM micrographs of co-assemblies of nonionic **PA1** and anionic **PA2** preserved in vitreous ice with the molar fraction of **PA2** in the co-assemblies indicated. (b) SAXS intensities of the co-assembled PA systems as a function of the wave vector with vertical lines showing the first minimum of the **PA1** and **PA2** scans. (c) WAXS intensity as a function of the wave vector for the co-assembled PA systems. (d) CD spectra as a function of wavelength for the co-assembled PA systems. (e) FTIR absorbance spectra as a function of wavenumber for the co-assembled PA systems with vertical line showing the peak absorbance in the amide I′ band for **PA1** and **PA2**.

copolymer, the system adopts a morphology that best minimizes charge repulsion. Thereafter, even as additional PA molecules are substituted for uncharged PA molecules, there is sufficient repulsion among the charged groups for the PA to maintain the morphology of the completely charged assembly.

Next, we investigated how changing the total charge of the supramolecular copolymers affected intermolecular order among molecules within the assemblies. Using wide-angle X-ray scattering (WAXS), we observed three peaks: the first at a d-spacing of 0.84 nm was a result of the (01) spacing between the β-sheets, the second peak with a *d*-spacing of 0.47 nm originates from the (10) spacing among molecules within the β-sheet, and the third peak corresponding to a *d*-spacing of 0.41 nm is a (11) reflection. The intensities of the (01) and (11) peaks were stronger in the fully nonionic supramolecular polymers than in the fully anionic assemblies. This may be explained by the long-range nature of electrostatic interactions, which would be greater than that of local steric interactions, so repulsion among ionic charges on neighboring β-sheets affected the spacing between the sheets. Thus, steric repulsion among PEG chains would be more likely to affect interactions among nearest neighbors only. Surprisingly, the strongest (10) peak occurred when **PA1** and **PA2** were mixed in an equimolar ratio, suggesting that the arrangement of molecules within the co-assemblies minimized repulsion among the molecules (Fig. 3c). Thus, while the change in supramolecular morphology with increasing charge was monotonic, the fraction of molecules with the characteristic β-sheet spacing first increased and then decreased with increasing **PA2** content. For co-assemblies of **PA1** and the cationic **PA3**, the intensity of all three peaks decreased with increasing charged PA content (Fig. S5b). While the lysine side chains affected assembled morphology less than glutamic acid residues, interactions among lysine groups in the same β-sheet may have had a stronger effect on hydrogen bonding along the filament axis than interactions among glutamic acid residues, possibly due to steric interactions as a result of the bulkier side chains.

We hypothesized that the strong (10) WAXS peak observed when **PA1** and **PA2** were co-assembled was a result of molecules within the filaments arranging to minimize repulsive interactions with their neighbors—both by limiting steric interactions among neighboring PEG chains and by limiting electrostatic interactions among nearby charged groups. We used CD spectroscopy to further probe the effects of co-assembly on interactions among the molecules within filaments. CD showed weaker overall β-sheet signal for **PA1** alone and co-assemblies containing 5 mol% **PA2** and the greatest intensities occurred in systems containing 25–75 mol% **PA2** (Fig. 3d), further supporting the result that co-assembling **PA1** and **PA2** increased β-sheet content relative to either PA alone. To further investigate this hypothesis, we used Fourier-transform infrared spectroscopy (FTIR) to monitor the amide I′ peak, which indicates β-sheet secondary structure.[46] We observed a shift in the peak to lower wavenumbers for **PA2** relative to the nonionic **PA1**. In co-assembled systems, the position of the amide I′ peak shifted from 1625 cm^{-1} to 1623 cm^{-1} with

the addition of 25 mol% **PA2** to **PA1** assemblies, but shifted only slightly more, to 1622 cm^{-1}, for 100 mol% **PA2** assemblies (Fig. 3e). Previous reports of alanine-rich peptides indicate that this shift correlates with hydration of the peptides,[47] suggesting increasing charge leads to greater internal hydration of the supramolecular filaments. These results point to the complementary ways in which combining charged and non-charged groups can strengthen hydrogen bonding interactions within the assemblies. Once a threshold fraction of charged **PA2** molecules was added to **PA1** assemblies, ordered lateral spacing between neighboring β-sheets decreased due to repulsion among charged groups, as evidenced by the decrease of the (01) WAXS peak. This in turn would increase the spacing between PEG segments on neighboring β-sheets, freeing more space for water to penetrate the filament and leading to more hydrated—and possibly more dynamic—assemblies. On the other hand, co-assembling nonionic **PA1** with anionic **PA2** can separate **PA2** molecules from one another within β-sheets, thus decreasing repulsive interactions among glutamic acid groups and yielding increased β-sheet content. Thus, we expect that co-assembling PA molecules with ionic and nonionic hydrophilic groups is a potential strategy to limit the repulsive interactions present in homogeneous β-sheet-forming assemblies.

Effect of surface charge on PA filament bioactivity

To test the biocompatibility of the nonionic **PA1**, we treated normal human lung fibroblast (nHLF) cultures with PA solutions of various concentrations. Both **PA1** and **PA2** were non-cytotoxic, with over 85% of cells staining positive for calcein at up to 100 μM PA, whereas **PA3** was highly cytotoxic (EC_{50} = 25 ± 4 μM). This trend is consistent with our previous reports, where cytotoxicity of cationic PA assemblies was attributed to disruption of the cell membrane. Thus, we demonstrated that **PA1** could provide an alternative to **PA3** for applications where negatively charged surfaces are undesirable, such as binding to receptors on the negatively charged cell membrane (Fig. 4a and Fig. S6). Because only **PA1** and **PA2** were non-toxic to the cell cultures, we chose to compare how they affect cell fate in additional experiments.

To determine the effect of charged and uncharged groups in PA copolymers on cellular function, we chose to study differentiation of mesenchymal stem cells (MSCs) as a model system, since these cells have previously been shown to respond to surface charge *in vitro*.[48] Specifically, osteogenic differentiation of MSC cultures is reported to be reduced by carboxylic acid functionalization and increased in response to amine group or hydroxyl group functionalization of gold nanoparticles[49] or titanium oxide nanorods,[50] due to upregulation of proliferative signals like transforming growth factor β (TGFβ) by acidic groups. Importantly, TGFβ signaling is necessary for the early stages of endochondral ossification,[51] meaning the effect of charged groups on *in vivo* bone formation may be more complex. While previous reports on the effect of nanomaterials' charge on osteogenic differentiation have focused on particles that present a single functional group, the supramolecular copolymers we report here provide a technique to present both charged and uncharged functional groups at a controlled ratio, making it possible to study how osteogenic progenitors respond to the presence of multiple functional groups in this *in vitro* model.

To determine the effect of nonionic and ionic groups in PA supramolecular copolymers on osteogenic differentiation, human MSCs were cultured in osteogenic media containing either no PA or **PA1**, **PA2**, or co-assemblies of the two PAs at 100 μM. Co-assemblies of these two PA molecules were assumed to be non-cytotoxic due to the well-known biocompatibility of the PA components; this was supported by the healthy cell morphology and density for cells treated with these copolymers. After 14 days *in vitro*, cells cultured in osteogenic media with or without the presence of PA exhibited a stellate morphology as opposed to the spindle morphology observed in cells maintained in the growth media used to expand the cultures (Fig. S7). To determine if the presence of PA filaments in human MSC cultures affected their phenotype, osteogenic

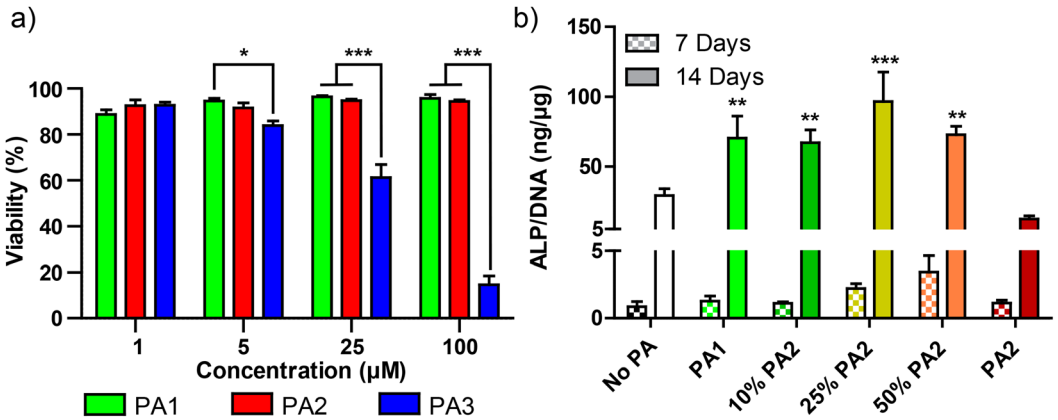

Fig. 4 (a) Percent viable cells as a function of PA concentration for nHLF cultures treated with **PA1**, **PA2**, or **PA3** for 36 h; significance calculated relative to other PA treatments at the same concentration (n = 3). (b) ALP activity normalized to DNA concentration for human MSCs treated with 100 μM **PA1** and **PA2** co-assemblies cultured in osteogenic media for 7 and 14 days; significance calculated relative to no PA control for each timepoint (n = 4). (*, $p < 0.05$; **, $p < 0.01$; ***, $p < 0.001$)

differentiation was quantified using an assay of alkaline phosphatase (ALP) activity after 7 days and after 14 days. After 7 days, ALP activity was generally low, with slightly higher activity observed in the presence of the PA copolymer containing 50% **PA1** and 50% **PA2** relative to the no PA control. After 14 days, PA treatment showed a significant effect on osteogenic differentiation. Relative to human MSC cultures without PA treatment, ALP activity was increased significantly in cultures treated with **PA1** alone and in cultures treated with supramolecular copolymers containing **PA1** and 10%, 25% or 50% **PA2**, but not in cultures treated with **PA2** only filaments. These results demonstrate that, similar to hydroxyl functionalized nanoparticles, the presentation of nonionic PEG groups by PA filaments can strongly affect cellular differentiation *in vitro*, significantly enhancing osteogenesis even in cells already primed for differentiation by osteogenic culture media. Importantly, as the ratio of **PA1** to **PA2** molecules decreased, ALP activity did not, suggesting that the presence of carboxylic groups did not diminish the osteogenic effect (Fig. 4b). Surprisingly, the greatest increase in ALP activity relative to the control without PA occurred in a co-assembly of 25 mol% **PA2** with 75 mol% **PA1**, rather than the treatment that included the highest concentration of PEG groups (Fig. 4b). Based on our characterization studies at this co-assembly ratio, the PA molecules formed more hydrated, ionic PA-like assemblies, while maintaining a high surface density of PEGylated groups. The increased space between PEG moieties in these co-assemblies can enhance their ability to bind proteins which signal cells to promote osteogenesis. Furthermore, PEG moieties and their hydration in the nonionic PA molecules can enhance supramolecular dynamics, which in turn is known to improve signaling capacity.[52,53] While exploring the effect of PA charge on osteogenesis *in vivo* is beyond the scope of this work, these results clearly show that the incorporation of nonionic PA molecules in co-assemblies would be useful for this purpose.

Conclusions

In this study, we report on supramolecular filaments of a nonionic PEGylated PA that polymerize into similar nanofilaments at acidic, neutral, and basic pH with limited sensitivity to buffer ionic strength. Co-polymerizing these nonionic PA molecules with charged monomers led to filaments with a tunable surface charge and demonstrated that only a minority of charged groups within an assembly produced nanostructures with a similar morphology to assemblies containing only charged PA molecules. Our results also show that nonionic PEGylated PA assemblies are biocompatible based on cell viability data and show an increase *in vitro* osteogenic differentiation in response to the filaments relative to untreated controls. Interestingly, we found that all supramolecular assemblies investigated containing PEGylated PA molecules have enhanced bioactivity relative to assemblies containing only charged PAs. We hypothesize that this effect originates in the synergistic effect of protein binding to PA molecules and enhanced supramolecular dynamics for cell signaling introduced by PEGylated molecules. We thus envision nonionic, filament-forming PA molecules as a useful tool in future studies of bioactivity in PA assemblies where surface charge plays an important role. For example, extending a fraction of the nonionic PA molecules within the filament with bioactive peptide sequences may enhance recognition of specific targets or decrease repulsive interactions with cell membranes to improve receptor binding.

Author contributions

J. A. L., R. F., N. S., and S. I. S. designed research; J. A. L, R. F., T. D. C., and J. M. G. performed experiments; J. A. L., R. F., and S. I. S. analyzed data; and J. A. L. and S. I. S. wrote the manuscript. All authors have given approval to the final version of the manuscript.

Conflicts of interest

There are no conflicts to declare.

Data availability

All study data are included in the article and/or supplementary information (SI). Supplementary information: Fig. S1: MS and LC-MS of PA molecules tested. Fig. S2: Nile Red assay for **PA3**. Fig. S3: Structure and zeta-potential measurements for **PA4** and **PA5**. Fig. S4: SAXS patterns and CD spectra for **PA4** and **PA5**. Fig. S5: SAXS and WAXS patterns for co-assemblies of **PA1** and **PA3**. Fig. S6: Live-dead images of nHLF cells treated with **PA1**, **PA2**, and **PA3**. Fig. S7: Fluorescent microscopy of MSCs treated with 100 μM PA. Table S1: Fitting parameters for Nile red study. See DOI: https://doi.org/10.1039/d6tb00293e.

Acknowledgements

This work was primarily supported by a gift from the Shannon Family Fund for Bio-Inspired and Bioactive Materials Systems for Musculoskeletal Regeneration. Additional support was provided by the National Science Foundation under award number DMR-2310178 (for transmission electron microscopy and electron scattering studies) and the Center for Regenerative Nanomedicine (CRN) of Northwestern University and by the National Institute of Dental and Craniofacial Research under grant number 5R01DE015920-07 (for biological studies). J. A. L. was supported by an NSF Graduate Research Fellowship (grant DGE-1324585). The authors thank Liam Palmer for his work editing the manuscript and Mark Karver of the Peptide Synthesis Core Facility in CRN for his assistance in purifying and characterizing the peptides. Peptide synthesis was performed at the Peptide Synthesis Core Facility and the chemical and biological characterization was performed at the Analytical BioNanoTechnology Core (ANTEC) in CRN. ANTEC (RRID:SCR_023706) receives partial support from the Feinberg School of Medicine,

Northwestern University. This work made use of the BioCryo facility (RRID:SCR_021288) of Northwestern University's NUANCE Center, which has received support from the International Institute for Nanotechnology (IIN) and Northwestern's MRSEC program (NSF DMR-2308691). Additional chemical characterization was performed at the Northwestern University Keck Biophysics Facility, which is supported by a Cancer Center Support Grant (NCI CA060553). X-ray experiments were performed at the DuPont-Northwestern-Dow Collaborative Access Team (DND-CAT) located at Sector 5 of the Advanced Photon Source (APS). DND-CAT is supported by Northwestern University, The Dow Chemical Company, and DuPont de Nemours, Inc. This research used resources of the Advanced Photon Source, a U.S. Department of Energy (DOE) Office of Science User Facility operated for the DOE Office of Science by Argonne National Laboratory under Contract No. DE-AC02-06CH11357. Additionally, this work made use of the IMSERC (RRID:SCR_017874) facility at Northwestern University, which has received support from the Soft and Hybrid Nanotechnology Experimental (SHyNE) Resource (NSF ECCS-1542205), the State of Illinois, and the IIN.

References

1 M. P. Monopoli, C. Aberg, A. Salvati and K. A. Dawson, Biomolecular coronas provide the biological identity of nanosized materials, *Nat. Nanotechnol.*, 2012, **7**(12), 779–786, DOI: 10.1038/nnano.2012.207.

2 M. Hadjidemetriou and K. Kostarelos, Nanomedicine: Evolution of the nanoparticle corona, *Nat. Nanotechnol.*, 2017, **12**(4), 288–290, DOI: 10.1038/nnano.2017.61.

3 E. Frohlich, The role of surface charge in cellular uptake and cytotoxicity of medical nanoparticles, *Int. J. Nanomed.*, 2012, **7**, 5577–5591, DOI: 10.2147/IJN.S36111.

4 S. G. Elci, Y. Jiang, B. Yan, S. T. Kim, K. Saha, D. F. Moyano, G. Yesilbag Tonga, L. C. Jackson, V. M. Rotello and R. W. Vachet, Surface Charge Controls the Suborgan Biodistributions of Gold Nanoparticles, *ACS Nano*, 2016, **10**(5), 5536–5542, DOI: 10.1021/acsnano.6b02086.

5 H.-X. Wang, Z.-Q. Zuo, J.-Z. Du, Y.-C. Wang, R. Sun, Z.-T. Cao, X.-D. Ye, J.-L. Wang, K. W. Leong and J. Wang, Surface charge critically affects tumor penetration and therapeutic efficacy of cancer nanomedicines, *Nano Today*, 2016, **11**(2), 133–144, DOI: 10.1016/j.nantod.2016.04.008.

6 A. S. Karakoti, S. Das, S. Thevuthasan and S. Seal, PEGylated inorganic nanoparticles, *Angew. Chem., Int. Ed.*, 2011, **50**(9), 1980–1994, DOI: 10.1002/anie.201002969.

7 J. S. Suk, Q. Xu, N. Kim, J. Hanes and L. M. Ensign, PEGylation as a strategy for improving nanoparticle-based drug and gene delivery, *Adv. Drug Delivery Rev.*, 2016, **99**(Pt A), 28–51, DOI: 10.1016/j.addr.2015.09.012.

8 M. J. Webber, E. A. Appel, B. Vinciguerra, A. B. Cortinas, L. S. Thapa, S. Jhunjhunwala, L. Isaacs, R. Langer and D. G. Anderson, Supramolecular PEGylation of biopharmaceuticals, *Proc. Natl. Acad. Sci. U. S. A.*, 2016, **113**(50), 14189–14194, DOI: 10.1073/pnas.1616639113.

9 Q. Dai, C. Walkey and W. C. Chan, Polyethylene glycol backfilling mitigates the negative impact of the protein corona on nanoparticle cell targeting, *Angew. Chem., Int. Ed.*, 2014, **53**(20), 5093–5096, DOI: 10.1002/anie.201309464.

10 A. D. Tagalakis, G. D. Kenny, A. S. Bienemann, D. McCarthy, M. M. Munye, H. Taylor, M. J. Wyatt, M. F. Lythgoe, E. A. White and S. L. Hart, PEGylation improves the receptor-mediated transfection efficiency of peptide-targeted, self-assembling, anionic nanocomplexes, *J. Controlled Release*, 2014, **174**, 177–187, DOI: 10.1016/j.jconrel.2013.11.014.

11 Q. Chen, S. Yu, D. Zhang, W. Zhang, H. Zhang, J. Zou, Z. Mao, Y. Yuan, C. Gao and R. Liu, Impact of Antifouling PEG Layer on the Performance of Functional Peptides in Regulating Cell Behaviors, *J. Am. Chem. Soc.*, 2019, **141**(42), 16772–16780, DOI: 10.1021/jacs.9b07105.

12 J. H. Collier and P. B. Messersmith, Self-Assembling Polymer–Peptide Conjugates: Nanostructural Tailoring, *Adv. Mater.*, 2004, **16**(11), 907–910, DOI: 10.1002/adma.200306379.

13 I. W. Hamley, I. A. Ansari, V. Castelletto, H. Nuhn, A. Rosler and H. A. Klok, Solution self-assembly of hybrid block copolymers containing poly(ethylene glycol) and amphiphilic beta-strand peptide sequences, *Biomacromolecules*, 2005, **6**(3), 1310–1315, DOI: 10.1021/bm049286g.

14 D. R. Perinelli, M. Campana, I. Singh, D. Vllasaliu, J. Doutch, G. F. Palmieri and L. Casettari, PEGylation affects the self-assembling behaviour of amphiphilic octapeptides, *Int. J. Pharm.*, 2019, **571**, 118752, DOI: 10.1016/j.ijpharm.2019.118752.

15 J. E. Goldberger, E. J. Berns, R. Bitton, C. J. Newcomb and S. I. Stupp, Electrostatic control of bioactivity, *Angew. Chem., Int. Ed.*, 2011, **50**(28), 6292–6295, DOI: 10.1002/anie.201100202.

16 S. Y. Qin, S. S. Xu, R. X. Zhuo and X. Z. Zhang, Morphology transformation via pH-triggered self-assembly of peptides, *Langmuir*, 2012, **28**(4), 2083–2090, DOI: 10.1021/la203518w.

17 F. Tantakitti, J. Boekhoven, X. Wang, R. V. Kazantsev, T. Yu, J. Li, E. Zhuang, R. Zandi, J. H. Ortony, C. J. Newcomb, L. C. Palmer, G. S. Shekhawat, M. Olvera de la Cruz, G. C. Schatz and S. I. Stupp, Energy landscapes and functions of supramolecular systems, *Nat. Mater.*, 2016, **15**(4), 469–476, DOI: 10.1038/nmat4538.

18 K. Sato, W. Ji, L. C. Palmer, B. Weber, M. Barz and S. I. Stupp, Programmable Assembly of Peptide Amphiphile via Noncovalent-to-Covalent Bond Conversion, *J. Am. Chem. Soc.*, 2017, **139**(26), 8995–9000, DOI: 10.1021/jacs.7b03878.

19 R. Xing, C. Yuan, S. Li, J. Song, J. Li and X. Yan, Charge-Induced Secondary Structure Transformation of Amyloid-Derived Dipeptide Assemblies from beta-Sheet to alpha-Helix, *Angew. Chem., Int. Ed.*, 2018, **57**(6), 1537–1542, DOI: 10.1002/anie.201710642.

20 G. Zaldivar, S. Vemulapalli, V. Udumula, M. Conda-Sheridan and M. Tagliazucchi, Self-Assembled Nanostructures of Peptide Amphiphiles: Charge Regulation by Size Regulation, *J. Phys. Chem. C*, 2019, **123**(28), 17606–17615, DOI: 10.1021/acs.jpcc.9b04280.

21 J. R. Wester, J. A. Lewis, R. Freeman, H. Sai, L. C. Palmer, S. E. Henrich and S. I. Stupp, Supramolecular Exchange

among Assemblies of Opposite Charge Leads to Hierarchical Structures, *J. Am. Chem. Soc.*, 2020, **142**(28), 12216–12225, DOI: 10.1021/jacs.0c03529.

22 M. M. Ouberai, A. L. G. Dos Santos, S. Kinna, S. Madalli, D. C. Hornigold, D. Baker, J. Naylor, L. Sheldrake, D. J. Corkill, J. Hood, P. Vicini, S. Uddin, S. Bishop, P. G. Varley and M. E. Welland, Controlling the bioactivity of a peptide hormone in vivo by reversible self-assembly, *Nat. Commun.*, 2017, **8**(1), 1026, DOI: 10.1038/s41467-017-01114-1.

23 J. Son, D. Kalafatovic, M. Kumar, B. Yoo, M. A. Cornejo, M. Contel and R. V. Ulijn, Customizing Morphology, Size, and Response Kinetics of Matrix Metalloproteinase-Responsive Nanostructures by Systematic Peptide Design, *ACS Nano*, 2019, **13**(2), 1555–1562, DOI: 10.1021/acsnano.8b07401.

24 T. J. Moyer, J. A. Finbloom, F. Chen, D. J. Toft, V. L. Cryns and S. I. Stupp, pH and amphiphilic structure direct supramolecular behavior in biofunctional assemblies, *J. Am. Chem. Soc.*, 2014, **136**(42), 14746–14752, DOI: 10.1021/ja5042429.

25 E. J. Chung, L. B. Mlinar, M. J. Sugimoto, K. Nord, B. B. Roman and M. Tirrell, In vivo biodistribution and clearance of peptide amphiphile micelles, *Nanomedicine*, 2015, **11**(2), 479–487, DOI: 10.1016/j.nano.2014.08.006.

26 C. Y. J. Lau, N. Benne, B. Lou, D. T. Braake, E. Bosman, N. van Kronenburg, M. Fens, F. Broere, W. E. Hennink and E. Mastrobattista, Tuning surface charges of peptide nanofibers for induction of antigen-specific immune tolerance: an introductory study, *J. Pharm. Sci.*, 2022, **111**(4), 1004–1011, DOI: 10.1016/j.xphs.2022.01.030.

27 L. Haines-Butterick, K. Rajagopal, M. Branco, D. Salick, R. Rughani, M. Pilarz, M. S. Lamm, D. J. Pochan and J. P. Schneider, Controlling hydrogelation kinetics by peptide design for three-dimensional encapsulation and injectable delivery of cells, *Proc. Natl. Acad. Sci. U. S. A.*, 2007, **104**(19), 7791–7796, DOI: 10.1073/pnas.0701980104.

28 S. Zhang, M. A. Greenfield, A. Mata, L. C. Palmer, R. Bitton, J. R. Mantei, C. Aparicio, M. Olvera de la Cruz and S. I. Stupp, A self-assembly pathway to aligned monodomain gels, *Nat. Mater.*, 2010, **9**(7), 594–601, DOI: 10.1038/nmat2778.

29 J. D. Hartgerink, E. Beniash and S. I. Stupp, Self-assembly and mineralization of peptide-amphiphile nanofibers, *Science*, 2001, **294**(5547), 1684–1688, DOI: 10.1126/science.1063187.

30 J. D. Hartgerink, E. Beniash and S. I. Stupp, Peptide-amphiphile nanofibers: a versatile scaffold for the preparation of self-assembling materials, *Proc. Natl. Acad. Sci. U. S. A.*, 2002, **99**(8), 5133–5138, DOI: 10.1073/pnas.072699999.

31 J. H. Ortony, C. J. Newcomb, J. B. Matson, L. C. Palmer, P. E. Doan, B. M. Hoffman and S. I. Stupp, Internal dynamics of a supramolecular nanofibre, *Nat. Mater.*, 2014, **13**(8), 812–816, DOI: 10.1038/nmat3979.

32 H. Cui, E. T. Pashuck, Y. S. Velichko, S. J. Weigand, A. G. Cheetham, C. J. Newcomb and S. I. Stupp, Spontaneous and x-ray-triggered crystallization at long range in self-assembling filament networks, *Science*, 2010, **327**(5965), 555–559, DOI: 10.1126/science.1182340.

33 J. C. Stendahl, M. S. Rao, M. O. Guler and S. I. Stupp, Intermolecular Forces in the Self-Assembly of Peptide Amphiphile Nanofibers, *Adv. Funct. Mater.*, 2006, **16**(4), 499–508, DOI: 10.1002/adfm.200500161.

34 A. Iscen and G. C. Schatz, Hofmeister Effects on Peptide Amphiphile Nanofiber Self-Assembly, *J. Phys. Chem. B*, 2019, **123**(32), 7006–7013, DOI: 10.1021/acs.jpcb.9b05532.

35 C. J. Newcomb, S. Sur, J. H. Ortony, O. S. Lee, J. B. Matson, J. Boekhoven, J. M. Yu, G. C. Schatz and S. I. Stupp, Cell death versus cell survival instructed by supramolecular cohesion of nanostructures, *Nat. Commun.*, 2014, **5**, 3321, DOI: 10.1038/ncomms4321.

36 J. A. Lewis, R. Freeman, J. K. Carrow, T. D. Clemons, L. C. Palmer and S. I. Stupp, Transforming growth factor β-1 binding by peptide amphiphile hydrogels, *ACS Biomater. Sci. Eng.*, 2020, **6**(8), 4551–4560, DOI: 10.1021/acsbiomaterials.0c00679.

37 S. Sur, F. Tantakitti, J. B. Matson and S. I. Stupp, Epitope topography controls bioactivity in supramolecular nanofibers, *Biomater. Sci.*, 2015, **3**(3), 520–532, DOI: 10.1039/c4bm00326h.

38 R. Freeman, M. Han, Z. Alvarez, J. A. Lewis, J. R. Wester, N. Stephanopoulos, M. T. McClendon, C. Lynsky, J. M. Godbe, H. Sangji, E. Luijten and S. I. Stupp, Reversible self-assembly of superstructured networks, *Science*, 2018, **362**(6416), 808–813, DOI: 10.1126/science.aat6141.

39 D. J. Toft, T. J. Moyer, S. M. Standley, Y. Ruff, A. Ugolkov, S. I. Stupp and V. L. Cryns, Coassembled cytotoxic and pegylated peptide amphiphiles form filamentous nanostructures with potent antitumor activity in models of breast cancer, *ACS Nano*, 2012, **6**(9), 7956–7965, DOI: 10.1021/nn302503s.

40 C. Chen, D. Wu, W. Fu and Z. Li, Peptide hydrogels assembled from nonionic alkyl-polypeptide amphiphiles prepared by ring-opening polymerization, *Biomacromolecules*, 2013, **14**(8), 2494–2498, DOI: 10.1021/bm4008259.

41 Y. Wan, Z. Wang, J. Sun and Z. Li, Extremely Stable Supramolecular Hydrogels Assembled from Nonionic Peptide Amphiphiles, *Langmuir*, 2016, **32**(30), 7512–7518, DOI: 10.1021/acs.langmuir.6b00727.

42 A. K. Kenworthy, K. Hristova, D. Needham and T. J. McIntosh, Range and magnitude of the steric pressure between bilayers containing phospholipids with covalently attached poly (ethylene glycol), *Biophys. J.*, 1995, **68**(5), 1921–1936, DOI: 10.1016/S0006-3495(95)80369-3.

43 M. C. A. Stuart, J. C. van de Pas and J. B. F. N. Engberts, The use of Nile Red to monitor the aggregation behavior in ternary surfactant-water-organic solvent systems, *J. Phys. Org. Chem.*, 2005, **18**(9), 929–934, DOI: 10.1002/poc.919.

44 G. R. Grimsley, J. M. Scholtz and C. N. Pace, A summary of the measured pK values of the ionizable groups in folded proteins, *Protein Sci.*, 2009, **18**(1), 247–251, DOI: 10.1002/pro.19.

45 H. Zhang, M. Yu, A. Song, Y. Song, X. Xin, J. Shen and S. Yuan, Modulating hierarchical self-assembly behavior of a peptide amphiphile/nonionic surfactant mixed system, *RSC Adv.*, 2016, **6**(11), 9186–9193, DOI: 10.1039/c5ra25437j.

46 J. Seo, W. Hoffmann, S. Warnke, X. Huang, S. Gewinner, W. Schollkopf, M. T. Bowers, G. von Helden and K. Pagel, An infrared spectroscopy approach to follow beta-sheet formation in peptide amyloid assemblies, *Nat. Chem.*, 2017, **9**(1), 39–44, DOI: 10.1038/nchem.2615.

47 S. Mukherjee, P. Chowdhury and F. Gai, Infrared study of the effect of hydration on the amide I band and aggregation properties of helical peptides, *J. Phys. Chem. B*, 2007, **111**(17), 4596–4602, DOI: 10.1021/jp0689060.

48 L. S. Tew, J. Y. Ching, S. H. Ngalim and Y. L. Khung, Driving mesenchymal stem cell differentiation from self-assembled monolayers, *RSC Adv.*, 2018, **8**(12), 6551–6564, DOI: 10.1039/c7ra12234a.

49 J. J. Li, N. Kawazoe and G. Chen, Gold nanoparticles with different charge and moiety induce differential cell response on mesenchymal stem cell osteogenesis, *Biomaterials*, 2015, **54**, 226–236, DOI: 10.1016/j.biomaterials.2015.03.001.

50 S. Shrestha, Z. Mao, Y. Fedutik and C. Gao, Influence of titanium dioxide nanorods with different surface chemistry on the differentiation of rat bone marrow mesenchymal stem cells, *J. Mater. Chem. B*, 2016, **4**(43), 6955–6966, DOI: 10.1039/c6tb02149b.

51 G. Chen, C. Deng and Y. P. Li, TGF-beta and BMP signaling in osteoblast differentiation and bone formation, *Int. J. Biol. Sci.*, 2012, **8**(2), 272–288, DOI: 10.7150/ijbs.2929.

52 Z. Álvarez, A. Kolberg-Edelbrock, I. Sasselli, J. Ortega, R. Qiu, Z. Syrgiannis, P. Mirau, F. Chen, S. Chin and S. Weigand, Bioactive scaffolds with enhanced supramolecular motion promote recovery from spinal cord injury, *Science*, 2021, **374**(6569), 848–856, DOI: 10.1126/science.abh3602.

53 S. C. Yuan, Z. Alvarez, S. R. Lee, R. Z. Pavlovic, C. Yuan, E. Singer, S. J. Weigand, L. C. Palmer and S. I. Stupp, Supramolecular motion enables chondrogenic bioactivity of a cyclic peptide mimetic of transforming growth factor-β1, *J. Am. Chem. Soc.*, 2024, **146**(31), 21555–21567, DOI: 10.1021/jacs.4c05170.